Segmentation of Renal Parenchymal Area from Ultrasound Images Using Level Set Evolution

Huixuan Wang, Jose E. Pulido, Yihua Song, Susan L. Furth, Changhe Tu, Caiming Zhang
Chunming Li* and Gregory E. Tasian*

***Abstract*—This paper presents a framework for segmentation of renal parenchymal area from ultrasound images based on a 2-step level set method. We used distance regularized level set evolution method to partition the kidney boundary, followed by region-scalable fitting energy minimization method to segment the kidney collecting system, and determined renal parenchymal area by subtracting the area of the collecting system from the gross kidney area. The proposed method demonstrated excellent validity and low inter-observer variability.**

I. Introduction

Some children with urologic disorders maintain preserved kidney function over time while others progress to end stage renal disease (ESRD) [1, 2, 3]. Improved methods to predict which children are at greatest risk for ESRD are essential to identify those most likely to benefit from therapeutic interventions that decrease progression of loss of kidney function [4, 5]. Renal parenchymal area (RPA), which is the net functional area of the kidney, is obtained by subtracting the area of the kidney collecting system (CS) from the gross kidney area. RPA is associated with the risk of ESRD, with smaller areas likely indicating a decreased nephron mass and an increased likelihood of ESRD over time [6]. Currently, RPA is measured manually, which is a time intensive process that is inherently prone to inter- and intra-observer variability. Our objective was to develop a semi-automated method of determining RPA in order to decrease the variability in RPA measurement and human resources needed to obtain these measurements.

Ultrasound (US) is extensively used in the evaluation of children and adults with many different diseases and anatomic anomalies. However, it is especially difficult to segment objects of interest due to the relatively poor quality of US images compared with acquisitions from computed tomography (CT) and magnetic resonance imaging (MRI). A great deal of segmentation work using US images focuses on active contours taking the speckle noise into consideration [7, 8, 9, 10]. Although texture or shape priors can be incorporated into active contours to guide the motion of contours to define the kidney boundary [8, 9, 10], these methods are not sufficient for delineating RPA because they do not take into account the variability in both the shape and the size of the CS which may be quite large in patients with urologic diseases.

In this paper, we present a framework to segment RPA from US images using a 2-step algorithm based on active contour models in a level set scheme. Specifically, we used distance regularized level set evolution method (DRLSE) [11] to partition the boundary of kidney, followed by region-scalable fitting energy minimization method (RSF) [12] to segment the CS within the kidney to determine RPA. We allowed user-interaction to initialize the active contour, which consequently helped guide the contour to converge at edges of objects in a few iterations. Furthermore, the proposed method appeared to be reliable and valid, with little intra- or inter-observer variability in RPA measurements and similar values obtained from the proposed framework and gold-standard manual measurements.

This paper is organized as follows. In Section II, we discuss work on defining level set functional preparing for segmentation of kidney and CS, respectively. We report on the experimental results of our framework comparing with manual segmentation in Section III. Conclusions are made in Section IV.

II. Level Set Formulation

A. DRLSE for Kidney Segmentation

In level set models, contours are embedded as zero level set of a level set function (LSF), and are driven toward the boundary of objects along with the evolution of LSF according to minimization of an energy functional. Let I be an image on a domain Ω, $\varphi(\Omega \to R)$ denote an LSF, and C

Research supported by the National Nature Science Foundation of China (61020106001).

Huixuan Wang is with School of Computer Science and Technology, Shandong University, Jinan, 250101 China (e-mail: huixuan.wangupenn@gmail.com).

Jose E. Pulido is with the Division of Urology at the University of Pennsylvania, Philadelphia, PA 19104 USA (e-mail: josepulid@gmail.com).

Yihua Song is with the Key Laboratory of Medical Image Computing Ministry of Education, Northeastern University, Shenyang, China (e-mail:yihua.song@uphs.upenn.edu).

Susan L. Furth is with the Departments of Pediatrics and Epidemiology at the University of Pennsylvania and with the Division of Nephrology at the Children's Hospital of Philadelphia, Philadelphia, PA 19104 USA (e-mail: furths@email.chop.edu).

Changhe Tu is with School of Computer Science and Technology, Shandong University, Jinan, 250101 China (e-mail: chtu@sdu.edu.cn).

Caiming Zhang is with School of Computer Science and Technology, Shandong University, Jinan, 250101 China (e-mail: czhang@sdu.edu.cn).

* Chunming Li (co-corresponding author and co-senior author) is with the Center for Biomedical Image Computing and Analytics, University of Pennsylvania, Philadelphia, PA 19104 USA (phone: +1 615 618 7651, e-mail: lchunming@gmail.com).

* Gregory Tasian (co-corresponding author and co-senior author) is with the Division of Urology and the Center for Pediatric Clinical Effectiveness, The Children's Hospital of Philadelphia, Philadelphia, PA 19104 USA (e-mail: TasianG@email.chop.edu).

denote the zero level set of ϕ. We define energy functional $\varepsilon(\phi)$ by

$$\varepsilon(\phi) = \mu P(\phi) + \lambda L(\phi) + \alpha A(\phi) \tag{1}$$

where μ, λ and α are coefficients of level set regularization term $P(\phi)$, length term $L(\phi)$ and area term $A(\phi)$, respectively.

$P(\phi)$, $L(\phi)$ and $A(\phi)$ are defined by

$$P(\phi) = \frac{1}{2}\int_{\Omega}\left(|\nabla\phi| - 1\right)^2 d\mathrm{x} \tag{2}$$

$$L(\phi) = \int_{\Omega} g\delta(\phi)|\nabla\phi|\, d\mathrm{x} \tag{3}$$

$$A(\phi) = \int_{\Omega} gH(-\phi) d\mathrm{x} \tag{4}$$

The edge indicator function g is defined by

$$g = \frac{1}{1+|\nabla G_{\sigma} * I|^2} \tag{5}$$

where G_{σ} is a Gaussian kernel with a standard deviation σ.

Using the regularization of the Heaviside function H_{ε} and the Dirac delta function δ_{ε}, we deduce the energy functional approximately expressed as

$$\begin{aligned}\varepsilon_{\varepsilon}(\phi) = \mu\int_{\Omega}\frac{1}{2}\left(|\nabla\phi| - 1\right)^2 d\mathrm{x} + \lambda\int_{\Omega} g\delta_{\varepsilon}(\phi)|\nabla\phi|\, d\mathrm{x} \\ + \alpha\int_{\Omega} gH_{\varepsilon}(-\phi) d\mathrm{x}\end{aligned} \tag{6}$$

Equation (6) can be minimized by the variational method and gradient flow:

$$\frac{\partial\phi}{\partial t} = \mu\left(\nabla^2\phi - \mathrm{div}\left(\frac{\nabla\phi}{|\nabla\phi|}\right)\right) + \lambda\delta_{\varepsilon}(\phi)\mathrm{div}\left(g\frac{\nabla\phi}{|\nabla\phi|}\right) + \alpha g\delta_{\varepsilon}(\phi) \tag{7}$$

with an initial $\phi(\mathrm{x},0) = \phi_0(\mathrm{x})$.

We evolve ϕ according to (7) with C evolving synchronously toward the kidney boundary, and eventually C will converge at the edge of the kidney. It is worthwhile to use edge based DRLSE to determine kidney boundary because region based models become unreliable due to the similarity between pixels from inside and outside of kidney. Next, we segment the CS via region based RSF.

B. RSF for CS Segmentation

Let I be an image, x and C be a point and a closed contour in the image domain Ω, respectively, Ω_1 denote the region outside C, and Ω_2 denote the region inside C.

We define energy functional $\varepsilon(\phi)$ by

$$\begin{aligned}\varepsilon(\phi, f_1, f_2) = \sum_{i=1}^{2}\lambda_i\int\left(\int K_{\sigma}(\mathrm{x}-\mathrm{y})I(\mathrm{y}) - f_i(\mathrm{x})^2 M_i(\phi(\mathrm{y}))d\mathrm{y}\right)d\mathrm{x} \\ + \nu|C + \mu P(\phi)\end{aligned} \tag{8}$$

with

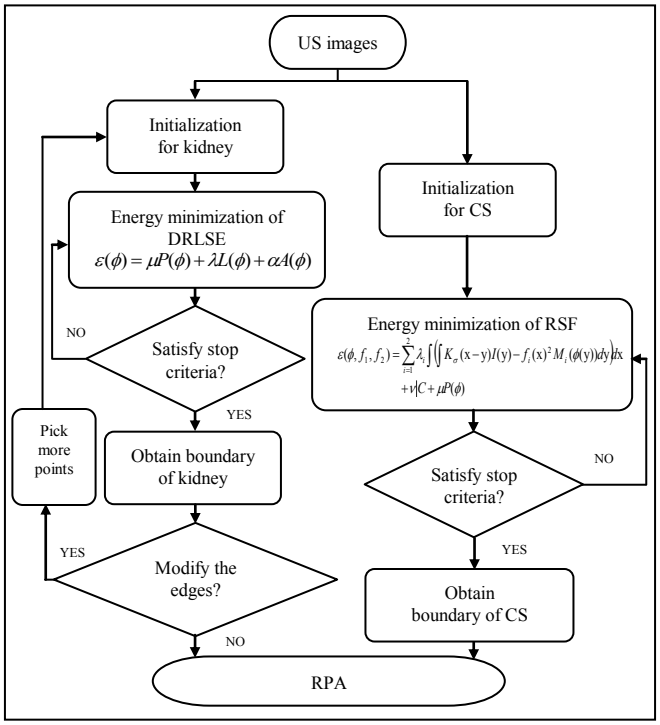

Figure 1. The proposed RPA segmentation framework.

$$M_1(\phi) = H(\phi)$$

$$M_2(\phi) = 1 - H(\phi)$$

where λ_1 and λ_2 are positive constants, $f_1(\mathrm{x})$ and $f_2(\mathrm{x})$ are values approximating image intensities in Ω_1 and Ω_2, respectively. In addition, $|C$ is the length of contour C, $P(\phi)$ is the level set regularization term, given by (3) and (2), respectively. In (8), the kernel function K plays a key role as the weight assigned to each image intensity $I(\mathrm{y})$ at y, and here is chosen as Gaussian kernel

$$K_{\sigma}(\mathrm{u}) = \frac{1}{(2\pi)^{n/2}\sigma^n} e^{-\mathrm{u}^2/2\sigma^2} \tag{9}$$

We introduce the Heaviside function H_{ε} and the Dirac delta function δ_{ε} to approximate the energy functional $\varepsilon(\phi, f_1, f_2)$ and minimize it with respect to ϕ keeping f_1 and f_2 fixed, consequently we obtain

$$\begin{aligned}\frac{\partial\varphi}{\partial t} = -\delta_{\varepsilon}(\varphi)(\lambda_1 e_1 - \lambda_2 e_2) + \nu\delta_{\varepsilon}(\varphi)div\left(\frac{\nabla\varphi}{|\nabla\varphi|}\right) \\ + \mu\left(\nabla^2\varphi - div\left(\frac{\nabla\varphi}{|\nabla\varphi|}\right)\right)\end{aligned} \tag{10}$$

with

$$e_i(\mathrm{x}) = \int K_{\sigma}(\mathrm{y}\text{-}\mathrm{x})\left|I(\mathrm{x}) \text{-} f_i(\mathrm{y})\right|^2 d\mathrm{y}, \quad i = 1,2$$

$$f_i(\mathrm{x}) = \frac{K_{\sigma}(\mathrm{x}) * \left[M_i(\phi)I(\mathrm{x})\right]}{K_{\sigma}(\mathrm{x}) * M_i(\phi)}, \quad i = 1,2$$

The motion of C will progress to the boundary of the CS with the evolution process of ϕ according to (10). Then RPA can be calculated by subtracting the area of the CS from the gross kidney area obtained before.

C. The RPA Segmentation Framework

Fig. 1 shows the proposed framework of RPA segmentation. First we use DRLSE to partition the kidney boundary, followed by RSF to segment the CS within kidney, and then RPA can be determined as a consequence. Minimal user-interaction is allowed to modify the shape of the kidney by picking more points to reinitialize the LSF. Letting users, especially experts, modify the shape of the kidney is an easy way to improve the accuracy of segmentation and extends the clinical applicability of this framework.

III. Experimental Results

We validated the proposed framework based on a random sample of 10 US images from 20 boys with a history of posterior urethral valves who were 6 months of age or younger at the time of presentation. The key parameters in the DRLSE model are μ, λ and α while the important parameters for the RSF model are λ_1, λ_2, ν, μ and σ. Unless otherwise specified, we set $\mu=0.2$, $\lambda=5.0$, $\alpha=-0.9$ in the first model, and $\lambda_1=1$, $\lambda_2=2$, $\nu=0.008*255*255$, $\mu=1$ and $\sigma=3$ in the other model.

A. Segmentation of RPA

The DRLSE model and RSF model have been applied to US images. Fig. 2 demonstrates the experimental results for a right kidney image of an infant. We used DRLSE and RSF model to partition the kidney border with brighter intensity and the CS with darker intensity, respectively. For this experiment, eight points were picked to outline the shape of the kidney coarsely while the boundary of the CS was initialized using squares centered at two selected points. Fig. 2 (c) shows the segmentation results of the kidney and the CS after 60 iterations under the proposed framework, while Fig. 2 (d) is the ground truth created by a urologist. We highlight RPA on Fig. 2 (e) and (f), respectively.

B. Measurements of RPA

We used the attribute PixelSpacing of DICOM files corresponding to US images to calculate the area of RPA. The first value of PixelSpacing is the spacing between the centers of adjacent rows in mm while the second value is the spacing between the centers of adjacent columns in mm. The area of RPA can be measured accurately as long as we obtain both the total number of pixels belonging to RPA and the values of PixelSpacing.

C. Validation of Intra-Observer Reliability

Using manual RPA segmentation as the gold standard, we determined the validity of the proposed framework:

$$SN = \frac{\left| M \bigcap A \right|}{\left| M \right|} \tag{11}$$

where M denotes the set of pixels within the manual segmentation by experts, A denotes the set of pixels obtained by the proposed method, and $|\cdot|$ denotes point set of segmentation results. We use SN to demonstrate the deviation from manual segmentation. The higher SN score, the closer the segmentation result obtained by the proposed method is to the manual segmentation result. A urologist (GET) manually measured RPA from 10 US images (Table I).

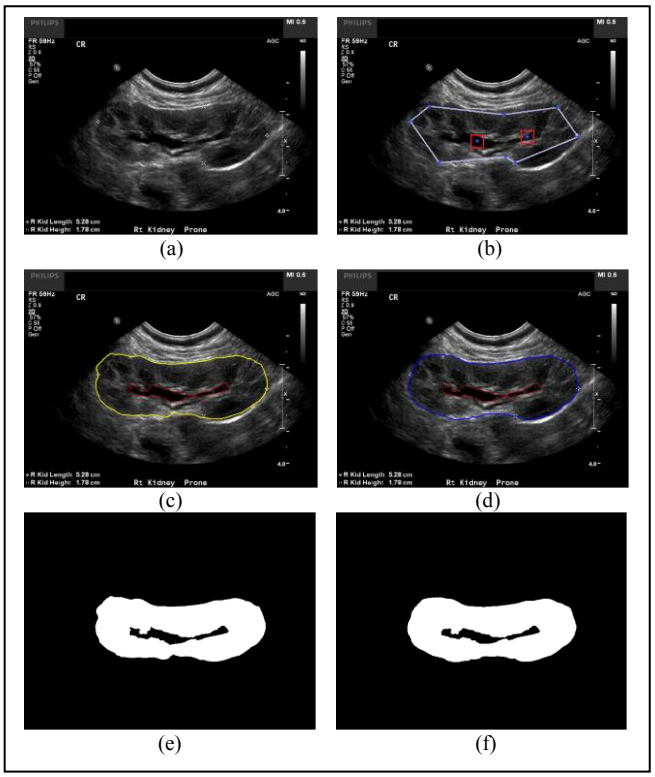

Figure 2. Experimental results on kidney and CS segmentation. (a) The test image. (b) Initialization of the segmentation process. (c) Segmentation result of the proposed method. (d) Manual segmentation result. (e) RPA obtained by the proposed method. (f) RPA obtained manually.

The quantitative results showed that our method was effective in segmenting RPA, with SN scores higher than 0.9 for all cases. Furthermore, different users obtained similar results with this method, showing its robustness to initialization.

However, the variability in RPA measurements between different users tended to be vulnerable with respect to test images with weak boundary conditions. For instance, on image 5 (Table I) user 1 obtained an increment by 4.76% compared with user 2 in SN score likely due to an unclear kidney border. Moreover, measurement precision could be improved by averaging the RPA of repeated experiments. We will conduct more extensive experiments in RPA measurements to further improve the proposed framework for clinical application.

IV. Conclusion

We present a framework to segment RPA from US images using a 2-step algorithm based on level set models. Specifically, we use DRLSE and RSF to segment the gross kidney area and CS, respectively, and then determine RPA by subtracting the area of the CS from the gross kidney area. User-interaction is allowed within the initialization of LSF to guide the process of evolution of LSF. The proposed method is accurate and reliable and is robust to variability in the points of initialization. This framework should extend the clinical applicability of RPA.

Acknowledgment

The work described in this paper is partly supported by a pilot grant awarded to Dr. Gregory Tasian from the Center for Pediatric Clinical Effectiveness at The Children's Hospital of Philadelphia.

TABLE I. Comparison of Measurement Results

Image Number	Method		RPA (square centimeter)	*SN*
1	The proposed framework	User 1	7.032	0.950
		User 2	6.918	0.964
	Manual segmentation		7.159	-
2	The proposed framework	User 1	9.565	0.928
		User 2	9.308	0.921
	Manual segmentation		8.964	-
3	The proposed framework	User 1	12.36	0.965
		User 2	11.89	0.932
	Manual segmentation		12.44	-
4	The proposed framework	User 1	17.53	0.972
		User 2	17.44	0.977
	Manual segmentation		17.29	-
5	The proposed framework	User 1	9.171	0.947
		User 2	8.790	0.904
	Manual segmentation		9.297	-
6	The proposed framework	User 1	11.46	0.914
		User 2	11.58	0.920
	Manual segmentation		11.92	-
7	The proposed framework	User 1	9.332	0.982
		User 2	9.335	0.985
	Manual segmentation		9.319	-
8	The proposed framework	User 1	8.108	0.943
		User 2	8.227	0.959
	Manual segmentation		7.897	-
9	The proposed framework	User 1	7.180	0.951
		User 2	6.943	0.966
	Manual segmentation		6.727	-
10	The proposed framework	User 1	9.189	0.972
		User 2	9.140	0.980
	Manual segmentation		9.135	-

References

[1] Dodson JL, Jerry-Fluker JV, Ng DK, et al, "Urological disorders in chronic kidney disease in children cohort: clinical characteristics and estimation of glomerular filtration rate," *J. Uroogyl.*, 2011, vol. 186, pp. 1460–1466.

[2] Gonzalez Celedon C, Bitsori M, Tullus K, "Progression of chronic renal failure in children with dysplastic kidneys," *Pediatr Nephrol*, 2007, vol. 22, pp. 1014-1020.

[3] Marra G, Oppezzo C, Ardissino G, et al, "Severe vesicoureteral reflux and chronic renal failure: a condition peculiar to male gender? Data from the ItalKid Project," *J. Pediatr*, 2004, vol. 144, pp. 677-681.

[4] Neild GH, "What do we know about chronic renal failure in young adults? II. Adult outcome of pediatric renal disease," *Pediatr Nephrol*, 2009, vol. 24, pp. 1921-1928.

[5] Neild GH, "What do we know about chronic renal failure in young adults? I. Primary renal disease," *Pediatr Nephrol*, 2009, vol. 24, pp. 1913-1919.

[6] Pulido JE, Furth SL, Zderic SA, Canning DA, Tasian GE, "Renal parenchymal area and risk of ESRD in boys with posterior urethral valves," *Clinical Journal of the American Society of Nephrology*, 2014, vol. 9, pp. 499-505.

[7] C. Davatzikos, R. Bryan, "Using a deformable surface model to obtain a shape representation of the cortex," *IEEE Trans. Med. Imag.*, 1996, vol. 15, pp. 785-795.

[8] Jun Xie, Yifeng Jiang, Hung-tat Tsui, "Segmentation of Kidney From Ultrasound Images Based on Texture and Shape Priors," *IEEE Trans. Med. Imag.*, 2005, vol. 24, pp. 45-57.

[9] Marcos Martin-Fernandez, Carlos Alberola-Lopez, "An approach for contour detection of human kidney from ultrasound images using Markov Random Fields and active contours," *Medical Image Analysis*, 2005, vol. 9, pp. 1-23.

[10] Fan Yang, Wenjian Qin, Yaoqin Xie, et al, "A shape-optimized Framework for kidney segmentation in ultrasound images using NLTV denoising and DRLSE," BioMedical Engineering Online, 2012, http://www.biomedical-engineering-online.com/content/11/1/82.

[11] Chunming Li, Chenyang Xu, Changfeng Gui, Martin D. Fox, "Distance Regularized level set evolution and its application to image segmentation," *IEEE Trans. Imag. Proc.*, 2010, vol. 19, pp. 3243-3254.

[12] Chunming Li, Chiu-Yen Kao, John C. Gore, Zhaohua Ding, "Minimization of region-scalable fitting energy for image segmentation," *IEEE Trans. Imag. Proc.*, 2008, vol. 17, pp. 1940-1949.